# Differential Regulation of Dynein and Kinesin Motor Proteins by Tau

Ram Dixit, *et al.*

*Science* **319**, 1086 (2008);
DOI: 10.1126/science.1152993



*Science* (print ISSN 0036-8075; online ISSN 1095-9203) is published weekly, except the last week in December, by the American Association for the Advancement of Science, 1200 New York Avenue NW, Washington, DC 20005. 

solutions orient the pentamer with its broader base facing outward. This is consistent with the role the pentamer appears to play in introducing curvature into the hexagonal layer. A notable feature of the hexagonal layer of the carboxysome shell is the presence of a bowl-shaped depression or concavity on one side of the hexameric building block (figs. S3 and S4). This depression is situated on the same side of the hexamer as both the N and C termini of the protein chain, and the prominence of the depression is affected by the disposition of the C terminus, which tends to vary in conformation between different homologs of the carboxysome hexamer (*11*, *12*). The narrow pore through the carboxysome hexamer tends to be positively charged, but the bowl-shaped depression surrounding the pore has a partial hydrophobic character, giving one side on the hexameric layer a distinctive appearance (Fig. 3). The model building does not resolve whether this side of the layer faces inward or outward. In one of the plausible models constructed here, it faces inward and could interact with RuBisCO, carbonic anhydrase, or possibly other protein components.

The present findings clarify the roles of previously uncharacterized proteins in the carboxysome; accordingly, we propose that the genes *orfA* and *orfB* be renamed *csoS4A* and *csoS4B*, consistent with other known shell protein genes in α-type carboxysomes. The results also lead to atomic models for the carboxysome shell, but these are incomplete in numerous respects, and considerably more work will be required to complete our understanding of this structure. For instance, the details of how the pentamers and hexamers fit together are only approximated here, and how the edges of the icosahedral shell are formed where a hexagonal layer bends is unknown. In addition, interactions that are almost certain to exist between the shell and the other enzymatic components of the carboxysome are only beginning to be elucidated (*28*).

The emerging structure of the carboxysome emphasizes common principles under which bacterial microcompartments and certain previously characterized viral capsids are constructed and illustrates the ability of evolution to produce a diversity of highly complex molecular structures from common principles and a small repertoire of basic building blocks. The elucidation of the component structures of the carboxysome shell also opens up strategies for designing new kinds of molecular containers or reaction chambers on the mid-nanometer scale.

### References and Notes


1. J. M. Shively, R. S. English, S. H. Baker, G. C. Cannon, *Curr. Opin. Microbiol.* **4**, 301 (2001).
2. M. R. Badger, G. D. Price, *J. Exp. Bot.* **54**, 609 (2003).
3. S. Heinhorst, G. C. Cannon, J. M. Shively, in *Complex Intracellular Structures in Prokaryotes*, J. M. Shively, Ed. (Springer, Berlin, 2006), vol. 2, pp. 141–165.
4. T. A. Bobik, *Appl. Microbiol. Biotechnol.* **70**, 517 (2006).
5. J. T. Penrod, J. R. Roth, *J. Bacteriol.* **188**, 2865 (2006).
6. J. M. Shively, F. L. Ball, B. W. Kline, *J. Bacteriol.* **116**, 1405 (1973).
7. E. Gantt, S. F. Conti, *J. Bacteriol.* **97**, 1486 (1969).
8. R. S. English, S. C. Lorbach, X. Qin, J. M. Shively, *Mol. Microbiol.* **12**, 647 (1994).
9. G. D. Price, S. M. Howitt, K. Harrison, M. R. Badger, *J. Bacteriol.* **175**, 2871 (1993).
10. A. K. So *et al.*, *J. Bacteriol.* **186**, 623 (2004).
11. C. A. Kerfeld *et al.*, *Science* **309**, 936 (2005).
12. Y. Tsai *et al.*, *PLoS Biol.* **5**, e144 (2007).
13. M. F. Schmid *et al.*, *J. Mol. Biol.* **364**, 526 (2006).
14. C. V. Iancu *et al.*, *J. Mol. Biol.* **372**, 764 (2007).
15. M. R. Badger, D. T. Hanson, G. D. Price, *Funct. Plant Biol.* **29**, 161 (2002).
16. J. M. Shively *et al.*, *Can. J. Bot.* **76**, 906 (1998).
17. G. C. Cannon *et al.*, *Appl. Environ. Microbiol.* **67**, 5351 (2001).
18. J. E. Johnson, J. A. Speir, *J. Mol. Biol.* **269**, 665 (1997).
19. D. L. Caspar, A. Klug, *Cold Spring Harbor Symp. Quant. Biol.* **27**, 1 (1962).
20. Materials and methods are available as supporting material on *Science* Online.
21. Z. Wunderlich *et al.*, *Proteins* **56**, 181 (2004).
22. E. Kofoid, C. Rappleye, I. Stojiljkovic, J. Roth, *J. Bacteriol.* **181**, 5317 (1999).
23. J. M. Shively, R. S. English, *Can. J. Bot.* **69**, 957 (1991).
24. J. T. Huiskonen, V. Manole, S. J. Butcher, *Proc. Natl. Acad. Sci. U.S.A.* **104**, 6666 (2007).
25. P. L. Stewart, R. M. Burnett, M. Cyrklaff, S. D. Fuller, *Cell* **67**, 145 (1991).
26. M. C. Lawrence, P. M. Colman, *J. Mol. Biol.* **234**, 946 (1993).
27. J. J. Gray *et al.*, *J. Mol. Biol.* **331**, 281 (2003).
28. B. M. Long, M. R. Badger, S. M. Whitney, G. D. Price, *J. Biol. Chem.* **282**, 29323 (2007).
29. See the Virus Particle Explorer, http://viperdb.scripps.edu/.


30. The authors thank D. Cascio for crystallographic advice and the staff at the Advanced Light Source beamline 8.2.2 for technical assistance. This work was supported by a grant from the Biological and Environmental Research program of the Department of Energy Office of Science. Support was also provided by NSF (grants MCB-0444568 and DMR-0213883 to G.C.C. and S.H., respectively). Protein structure coordinates and structure factors have been deposited in the Protein Data Bank (PDB); accession numbers are 2QW7 (CcmL), 2RCF (OrfA or CsoS4A), and 3BN4 (CcmK1).


### Supporting Online Material

www.sciencemag.org/cgi/content/full/319/5866/1083/DC1
Materials and Methods
SOM Text
Figs. S1 to S4
Tables S1 and S2
References

9 October 2007; accepted 3 January 2008
10.1126/science.1151458

# Differential Regulation of Dynein and Kinesin Motor Proteins by Tau

**Ram Dixit, Jennifer L. Ross,* Yale E. Goldman, Erika L. F. Holzbaur†**

**Dynein and kinesin motor proteins transport cellular cargoes toward opposite ends of microtubule tracks. In neurons, microtubules are abundantly decorated with microtubule-associated proteins (MAPs) such as tau. Motor proteins thus encounter MAPs frequently along their path. To determine the effects of tau on dynein and kinesin motility, we conducted single-molecule studies of motor proteins moving along tau-decorated microtubules. Dynein tended to reverse direction, whereas kinesin tended to detach at patches of bound tau. Kinesin was inhibited at about a tenth of the tau concentration that inhibited dynein, and the microtubule-binding domain of tau was sufficient to inhibit motor activity. The differential modulation of dynein and kinesin motility suggests that MAPs can spatially regulate the balance of microtubule-dependent axonal transport.**

Active transport of cytoplasmic material along microtubules is critical for cell organization and function, and defects in this process are associated with dysfunction and disease (*1*). Much of the active transport in cells depends on the molecular motor proteins cytoplasmic dynein and kinesin-1, which transport cargo toward the minus-end (toward the cell center) and plus-end of microtubules (toward the cell periphery), respectively. Dynein and kinesin have very different structures and translocation mechanisms (*2*). Kinesin has a compact motor domain and walks unidirectionally along single protofilaments with 8-nm steps (*2*). In contrast, dynein has a larger, more complex motor domain and is capable of variable step sizes, lateral steps across the microtubule surface, and processive runs toward both the minus- and plus-end of the microtubule (*3*–*5*). Cytoplasmic dynein function in vivo also requires an accessory complex, dynactin. This large, multiprotein complex is thought to facilitate dynein processivity (*6*) and may also regulate dynein activity (*5*). Within the cell, the balance between oppositely directed transport determines the steady-state distribution of organelles and biomolecules.

In the crowded cell environment, dynein and kinesin compete with nonmotile microtubule-associated proteins (MAPs) for binding to the microtubule surface. MAPs bound to microtubules might also block the path of motor proteins. Thus, MAPs can provide spatio-

Department of Physiology and Pennsylvania Muscle Institute, University of Pennsylvania, Philadelphia, PA 19104, USA.

*Present address: 302 Hasbrouck Laboratory, Department of Physics, University of Massachusetts at Amherst, Amherst, MA 01003, USA.

†To whom correspondence should be addressed. E-mail: holzbaur@mail.med.upenn.edu

temporal regulation of motor proteins in vivo. Tau, a neuronal MAP, inhibits kinesin activity in vivo and in vitro (*7*–*10*); however, its effect on dynein activity is not well understood. We sought to directly observe individual encounters between single dynein or kinesin motors and tau on microtubule tracks to determine how structurally distinct motors respond to obstacles in their path.

Tau is expressed in neurons as multiple splice forms in a developmentally regulated manner (*11*). These isoforms differ in the number of microtubule-binding repeats and the length of the projection domain (Fig. 1A). We focused on the shortest and longest tau isoforms, tau23 and tau40, to compare their overall effects on motor proteins. To directly visualize tau on microtubules, we fluorescently tagged purified recombinant tau proteins with Alexa 546 dye (fig. S1A). Functionality of labeled tau was demonstrated in microtubule-binding assays (fig. S2).

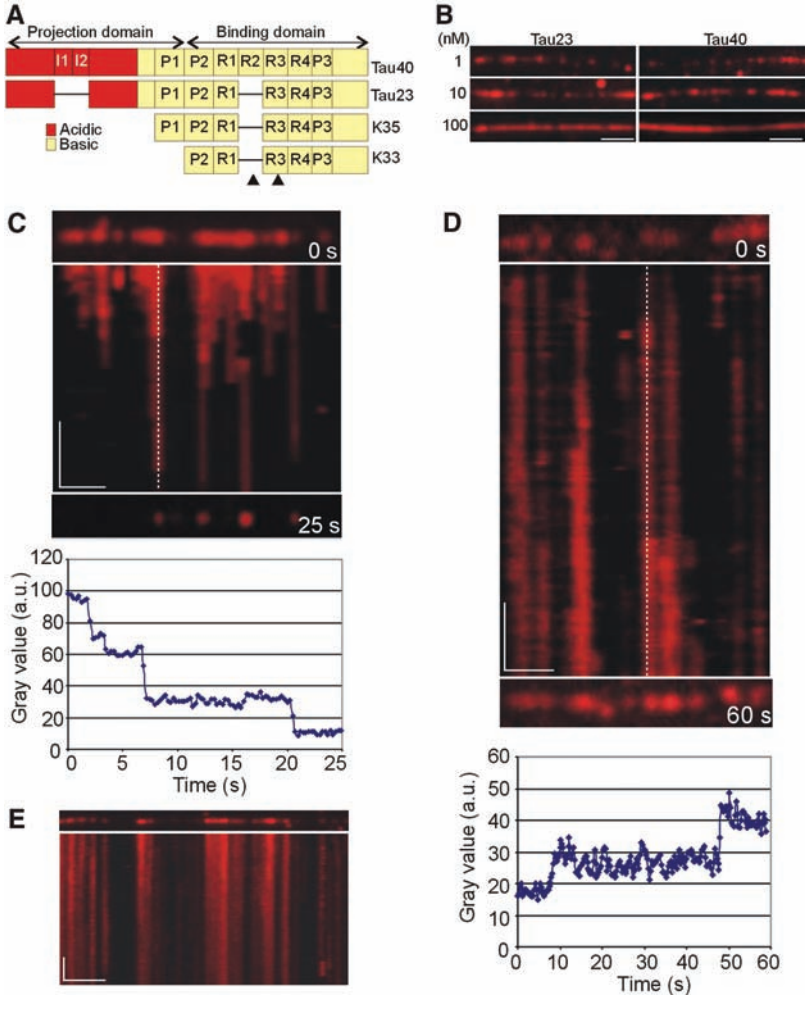


**Fig. 1.** Decoration of microtubules by Alexa-labeled tau. (**A**) Tau structure consists of an acidic projection domain and a basic microtubule-binding domain containing microtubule-binding repeats (R1 to R4) and proline-rich regions (P1 to P3). In the mammalian central nervous system, tau40 is the longest isoform and tau23 is the shortest isoform, which lacks insertions (I1 and I2) in the projection domain and the R2 microtubule-binding motif. K35 and K33 are recombinant variants of tau23 that are truncated at their N termini. Arrowheads indicate the position of cysteine residues used for conjugation of Alexa546. (**B**) Microtubule labeling by Alexa-tau23 and Alexa-tau40 shows a concentration-dependent increase in patch size and fluorescence intensity. Scale bars in (B) denote 2 μm. (**C**) Photobleaching of 10 nM Alexa-tau23 patches with a laser intensity 10 times as great as that used in (D) and (E) shows stepwise decreases in fluorescence intensity of the tau patches. Fluorescence intensity along the dotted line is plotted below, indicating four Alexa-tau23 molecules at this position. (**D**) Binding of 10 nM Alexa-tau23 to a microtubule shows a stepwise increase in fluorescence intensity of the tau patches. Fluorescence intensity along the dotted line is plotted below, showing sequential addition of two Alexa-tau23 molecules. (**E**) Kymograph shows stable tau decoration during the observation period. *x*-scale bar, 2 μm; *y*-scale bar, 10 s.

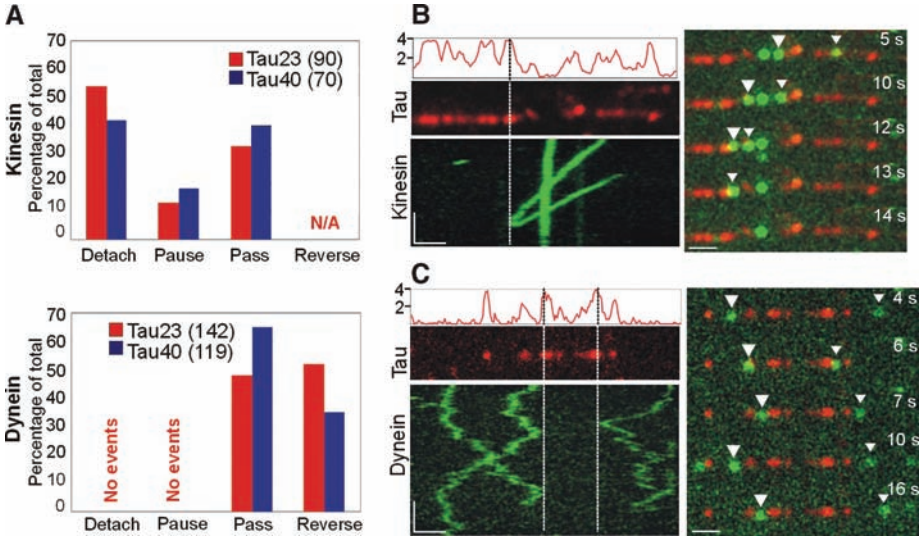


**Fig. 2.** Direct observation of encounters between single molecules of kinesin or dynein-dynactin and Alexa-labeled tau. (**A**) The effect of Alexa-tau23 (red bars) and Alexa-tau40 (blue bars) on kinesin and dynein motility. Kinesin either detaches, passes, or pauses (stationary for ≥ 10 frames) at a tau patch, whereas dynein either reverses direction or passes through a tau patch. The number of events is indicated in parentheses. (**B** and **C**) (Left) An Alexa-tau–decorated microtubule (red), with the relative intensity of tau fluorescence reported as the estimated number of tau molecules on the *y* axis. The kymograph (green) shows dissociation of two kinesin molecules (B) or directional reversal of two dynein-dynactin molecules (C) upon encountering a tau cluster (dotted line). (Right) Select images from each experiment. The arrowheads mark the kinesin or dynein molecules that encountered tau. *x*-scale bar, 1 μm; *y*-scale bar, 5 s. Scale bars in the right panels denote 1 μm.

Alexa-labeled tau23 and tau40 decorated Taxol-stabilized microtubules in patches whose size and fluorescence intensity increased with tau concentration (Fig. 1B). At 10 nM tau, patches were composed of 3 to 20 labeled tau molecules. Analysis of the spatial frequency spectrum of fluorescence intensity along the microtubule suggested that tau patches typically extended up to 1.2 μm (see legend to fig. S4). At peak intensity within a patch, we observed four or five bleaching events (Fig. 1C), corresponding to ~10 total tau molecules per diffraction-limited spot. These patches were formed by stepwise association of single tau molecules (Fig. 1D), consistent with tau's property of self-associating into clusters along the microtubule surface (*12*). The low–ionic strength buffer used in our experiments may fa-

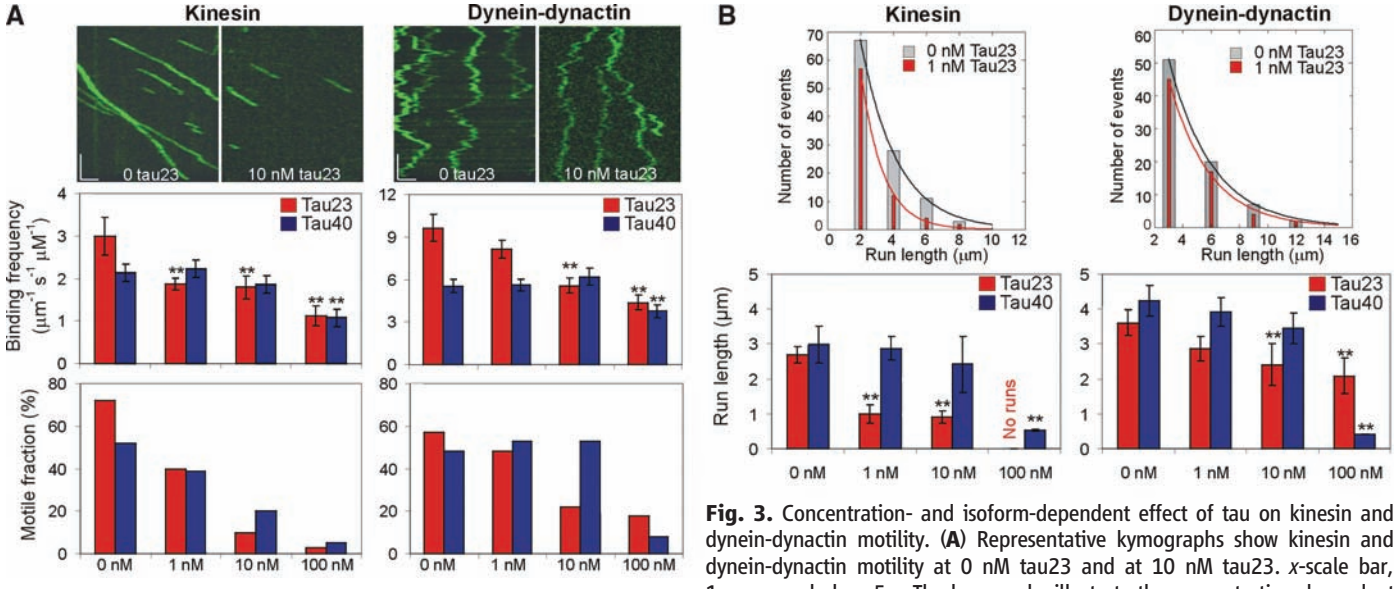


**Fig. 3.** Concentration- and isoform-dependent effect of tau on kinesin and dynein-dynactin motility. (**A**) Representative kymographs show kinesin and dynein-dynactin motility at 0 nM tau23 and at 10 nM tau23. *x*-scale bar, 1 μm; *y*-scale bar, 5 s. The bar graphs illustrate the concentration-dependent effect of tau23 (red bars) and tau40 (blue bars) on the average binding frequency and motile fraction of kinesin and dynein-dynactin. The error bars represent the SEM of ≥ 100 events for 0 to 10 nM tau and the SEM of ~50 events for 100 nM tau. A statistically significant difference ($P < 0.05$) from control is indicated by asterisks. (**B**) The histograms show the differential effect of 1 nM tau23 (orange bars) on the run length distribution of kinesin and dynein-dynactin. The bar graphs illustrate the concentration-dependent effects of tau23 (red bars) and tau40 (blue bars) on the average run length of kinesin and dynein-dynactin. The error bars represent the SEM of ≥ 100 events for 0 to 10 nM tau and the SEM of ~30 events for 100 nM tau. A statistically significant difference ($P < 0.05$) from control is indicated by asterisks.

**Fig. 4.** Comparison of the inhibitory effect of full-length and truncated versions of tau23 on kinesin and dynein-dynactin motility. (**A**) The bar graphs illustrate the effect of 0 nM (yellow bars), 10 nM (orange bars) and 25 nM (red bars) tau23 and its truncation variants, K35 and K33, on the average binding frequency and percent motile fraction of kinesin and dynein-dynactin. The error bars represent the SEM of ≥ 50 events. A statistically significant difference ($P < 0.05$) from control is indicated by asterisks. (**B**) Model of the role of tau in the regulation of axonal transport. In a healthy neuron, tau can be distributed in a proximal-distal gradient (shown in gray) that allows kinesin-driven anterograde transport from the cell body (green arrow). At the synapse, the relatively high tau concentration facilitates kinesin dissociation (red arrow). However, dynein is able to bind to distal microtubules because of its lower sensitivity to tau. In Alzheimer's disease (degenerating neuron), tau accumulates at the soma and consequently inhibits kinesin-driven anterograde transport (red blocked arrow), leading to neurodegeneration.

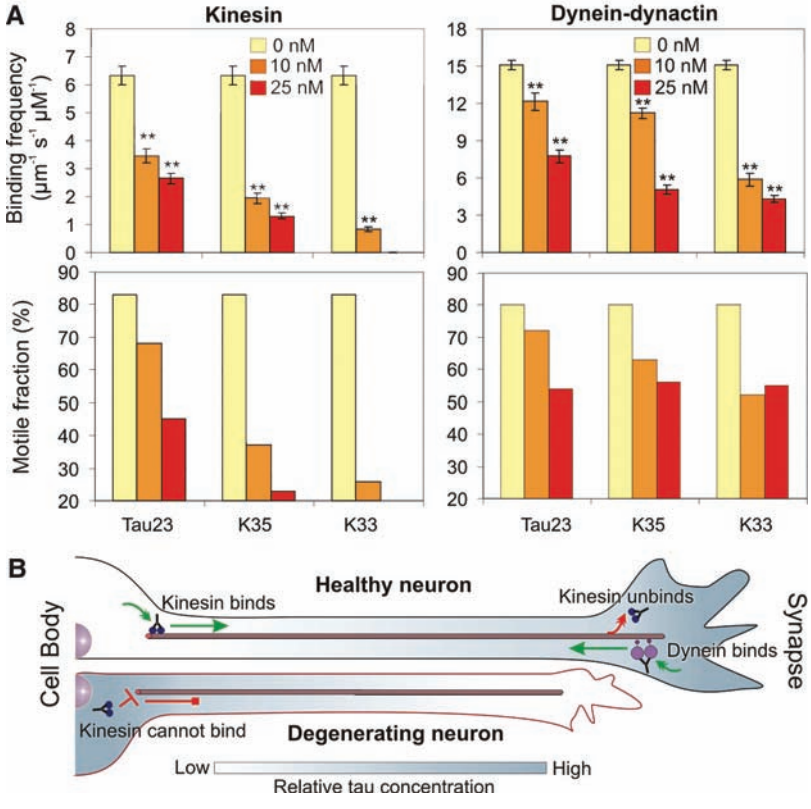

cilitate tau clustering, but concentration-dependent tau clustering has also been observed along axons in cultured neurons (*13*). Under the conditions of our experiments, the Alexa-tau patches were stable over the time course of several minutes (Fig. 1E), significantly longer than the average duration of motor runs (5 to 30 s). This feature allowed the direct visualization of encounters between motors and tau molecules bound to the microtubule surface.

Interactions between green fluorescent protein (GFP)-labeled dynein-dynactin isolated from mouse brain (*5*) or recombinant kinesin-GFP (*14*) (fig. S1, B and C) and Alexa-labeled tau on microtubules were observed directly by total internal reflection fluorescence microscopy (*5*). The frequency of kinesin-GFP binding to microtubules decreased with increasing local tau fluorescence intensity, whereas the frequency of dynein-dynactin-GFP binding was nearly independent of local tau fluorescence intensity (fig. S3). Thus, kinesin-GFP binding was inhibited more effectively by tau than was dynein-dynactin-GFP binding.

When single kinesin-GFP motors encountered tau patches on the microtubule, most of the motors detached from the microtubule surface (Fig. 2, A and B, and movies S1 and S2). For a given tau patch, kinesin was likely to detach at the position of peak tau fluorescence intensity (Fig. 2B). Hence, the probability of kinesin detachment is a function of the local tau concentration. Inhibition of kinesin motility was also tau-isoform specific. When kinesin-GFP did bind within a tau23 patch, mean run length was reduced by ~50% compared to mean run length along bare microtubule regions (from 1.7 ± 0.25 μm to 0.9 ± 0.03 μm; $n \geq 100$). Although tau40 patches also induced detachment of kinesin-GFP molecules (Fig. 2A and movie S2), the mean run length of kinesin-GFP moving within tau40 patches was not affected significantly (1.89 ± 0.36 μm; $n = 51$).

In contrast to kinesin, encounters of dynein-dynactin-GFP with Alexa-tau molecules did not induce motor detachment or pausing. Instead, dynein-dynactin tended to reverse direction upon encountering tau (Fig. 2, A and C, and movies S3 and S4). When dynein-dynactin bound within a tau23 patch, it did not rapidly detach like kinesin, but remained paused for relatively long periods (3 to 15 s). Tau40 also induced directional reversals as dynein-dynactin approached tau patches (Fig. 2A); however, the velocity and run length of dynein-dynactin within an Alexa-tau40 patch were not affected significantly (movie S4).

Thus, dynein-dynactin's response to encounters with tau was fundamentally different from kinesin's response, which may be related to dynein-dynactin's innate ability to execute processive backward runs. This ability would allow dynein-dynactin to remain attached to the microtubule after encounters with tau, whereas kinesin's inflexible nature makes it more likely to detach from the microtubule.

To examine the concentration-dependent effect of tau on motor function, we varied unlabeled tau23 and tau40 over a range encompassing the normal endogenous molar ratio of tubulin:tau of ~20:1. Tau decreased the binding frequency, motile fraction (defined as the proportion of landing motors that moved ≥250 nm), and run length of both kinesin-GFP and dynein-dynactin-GFP in a concentration- and isoform-dependent manner (Fig. 3, A and B; movies S5 to S10). The inhibitory effects of tau23 were less pronounced for dynein-dynactin than for kinesin. For example, 1 nM tau23 (50:1 tubulin: tau molar ratio) inhibited significantly the binding frequency and run length of kinesin but not of dynein-dynactin (Fig. 3). Significant inhibition of dynein was not observed until tau23 concentration was increased 10-fold. Tau40 was a less potent inhibitor for both motors; we did not obtain significant inhibition of either kinesin or dynein-dynactin motility at physiologically relevant tubulin:tau molar ratios with this isoform (Fig. 3). Neither tau23 nor tau40 significantly changed motor velocity of either kinesin or dynein-dynactin at any of the concentrations tested (table S1).

From a structural standpoint, tau might inhibit motor function through its projection domain and/or its microtubule-binding domain. To determine the relative contribution of these domains to motor inhibition, we studied the effects of truncated versions of tau23 on motor function. The truncated polypeptides, designated K35 and K33, differ in the length of their projection domain (Fig. 1A) but have microtubule-binding affinities similar to that of full-length tau23 (*15*). Alexa-labeled K35 and K33 decorated microtubules in a pattern similar to that observed for Alexa-labeled tau23 (fig. S4). The truncated forms of tau inhibited both kinesin-GFP and dynein-dynactin-GFP in a concentration-dependent manner (Fig. 4A). Indeed, both truncated forms were stronger inhibitors of motor proteins than was full-length tau23. Thus, the microtubule-binding domain of tau was sufficient for motor inhibition. Differences in the net charge of the projection domain between tau40 (−15), tau23 (−4), and K35 (+5) correlate well with their relative ability to inhibit binding of motor proteins, suggesting that the acidic projection domain may mimic the acidic tail of tubulin and electrostatically recruit motor proteins to the microtubule surface.

We propose a model in which tau controls the balance of microtubule-dependent axonal transport in the neuron by locally modulating motor function. In a healthy neuron, tau can be distributed in a proximal-to-distal gradient (*16*, *17*). Lower tau concentration at the cell body would allow kinesin to efficiently bind to microtubules and initiate anterograde transport of cargo, whereas higher tau concentration at the synapse would facilitate cargo release (Fig. 4B). At the same time, dynein-driven retrograde transport from the distal axon would not be impeded due to dynein's lower sensitivity to tau (Fig. 4B). Neurons can potentially fine-tune the occupancy of tau along axons by phosphorylation or dephosphorylation of sites within the microtubule-binding domain (*18*). On the basis of this model, perturbing tau distribution would predictably impair axonal transport. For example, in Alzheimer's disease, tau accumulates in the somatodendritic compartment (*19*, *20*); our model then predicts that kinesin-driven anterograde transport of new material to the axon terminal would be severely compromised, leading to neurodegeneration (*1*). The differential sensitivity of dynein and kinesin to tau thus provides a mechanism for spatiotemporal regulation of axonal transport.

### References and Notes


1. E. Chevalier-Larsen, E. L. Holzbaur, *Biochim. Biophys. Acta* **1762**, 1094 (2006).
2. R. D. Vale, *Cell* **112**, 467 (2003).
3. R. Mallik, B. C. Carter, S. A. Lex, S. J. King, S. P. Gross, *Nature* **427**, 649 (2004).
4. Z. Wang, M. P. Sheetz, *Cell Struct. Funct.* **24**, 373 (1999).
5. J. L. Ross, K. Wallace, H. Shuman, Y. E. Goldman, E. L. F. Holzbaur, *Nat. Cell Biol.* **8**, 562 (2006).
6. S. J. King, T. A. Schroer, *Nat. Cell Biol.* **2**, 20 (2000).
7. A. Ebneth *et al.*, *J. Cell Biol.* **143**, 777 (1998).
8. B. Trinczek, A. Ebneth, E. M. Mandelkow, E. Mandelkow, *J. Cell Sci.* **112**, 2355 (1999).
9. A. Seitz *et al.*, *EMBO J.* **21**, 4896 (2002).
10. M. Vershinin, B. C. Carter, D. S. Razafsky, S. J. King, S. P. Gross, *Proc. Natl. Acad. Sci. U.S.A.* **104**, 87 (2007).
11. A. Andreadis, *Prog. Mol. Subcell. Biol.* **44**, 89 (2006).
12. M. Ackmann, H. Wiech, E. Mandelkow, *J. Biol. Chem.* **275**, 30335 (2000).
13. S. Konzack, E. Thies, A. Marx, E. M. Mandelkow, E. Mandekow, *J. Neurosci.* **27**, 9916 (2007).
14. R. D. Vale *et al.*, *Nature* **380**, 451 (1996).
15. N. Gustke, B. Trinczek, J. Biernat, E. M. Mandelkow, E. Mandelkow, *Biochemistry* **33**, 9511 (1994).
16. M. Kempf, A. Clement, A. Faissner, G. Lee, R. Brandt, *J. Neurosci.* **16**, 5583 (1996).
17. M. M. Black, T. Slaughter, S. Moshiach, M. Obrocka, I. Fischer, *J. Neurosci.* **16**, 3601 (1996).
18. C. Ballatore, V. M.-Y. Lee, J. Q. Trojanowski, *Nat. Rev. Neurosci.* **8**, 663 (2007).
19. S. Khatoon, I. Grundke-Iqbal, K. Iqbal, *J. Neurochem.* **59**, 750 (1992).
20. H. Braak, E. Braak, E. M. Mandelkow, *Acta Neuropathol. (Berl.)* **87**, 554 (1994).


21. We thank E. Mandelkow for the tau constructs, R. Kudaravalli for purified kinesin, S. Shah for data analysis, and M. Ostap and members of the Holzbaur and Goldman labs for helpful comments. This work was supported by NIH grants P01-AR-051174 to the Pennsylvania Muscle Institute and GM-48661 to E.L.F.H., and NSF grant NSEC DMR04-25780 to the Penn Nano/Bio Interface Center.


### Supporting Online Material

www.sciencemag.org/cgi/content/full/1152993/DC1
Materials and Methods
Figs. S1 to S4
Table S1
References
Movies S1 to S10


14 November 2007; accepted 3 January 2008
Published online 17 January 2008;
10.1126/science.1152993
Include this information when citing this paper.